

Joseph J. Mallon, Joseph C. Uht, and Carol S. Hemminger
The Aerospace Corporation
2350 E. El Segundo Blvd.
El Segundo, CA 90245
Phone: 310/336-1619, Fax: 310/336-5846

ABSTRACT

We have conducted a series of surface analyses on carbon fiber/poly(arylacetylene) (PAA) matrix composites that were exposed to the space environment on the Long Duration Exposure Facility (LDEF) satellite. These composite panels were arranged in pairs on both the leading edge and trailing edge of LDEF. None of the composites were catastrophically damaged by nearly six years of exposure to the space environment. Composites on the leading edge exhibited from 25 to 125 μm of surface erosion, but trailing edge panels exhibited no physical appearance changes due to exposure. Scanning electron microscopy (SEM) was used to show that the erosion morphology on the leading edge samples was dominated by crevasses parallel to the fibers with triangular cross sections 10 to 100 μm in depth. The edges of the crevasses were well defined and penetrated through both matrix and fiber. The data suggest that the carbon fibers are playing an important role in crevasse initiation and/or enlargement, and in the overall erosion rate of the composite. X-ray photoelectron spectroscopy (XPS) and energy dispersive X-ray spectroscopy (EDS) results showed contamination from in-flight sources of silicone.

INTRODUCTION

LDEF experiment M0003, Space Environment Effects on Spacecraft Materials, consisted of 19 subexperiments and was flown as part of the materials, coatings, and thermal systems experimental category (ref. 1). The overall objective of this experiment was to obtain data concerning structure and property changes in materials that had been exposed to the space environment and to understand the reasons for these changes. Subexperiment M0003-16, Advanced Composite Materials, included three pairs of carbon fiber/poly(arylacetylene) (PAA) composite panels. Composites are principally used in space as structural components, so the effects of the space environment on the mechanical and physical properties of the composites flown on LDEF is of great interest to the design community. In this paper, we will report on the surface analyses of the carbon fiber/PAA composite samples as determined by optical microscopy, scanning electron microscopy (SEM), energy dispersive X-ray (EDS) spectroscopy, and X-ray photoelectron spectroscopy (XPS). Surface morphology changes due to space environment exposure and in-flight surface contamination will be discussed.

EXPERIMENTAL

Samples

The three composites selected for the experiment were carbon-fabric-reinforced poly(arylacetylene) (PAA) materials that were under development at The Aerospace Corporation in 1984 as replacements for more traditional composites such as carbon/epoxy. PAA is a hydrophobic matrix made by the

* This work was supported by Air Force Space Systems Division contract F04701-88-C-0089.

polycyclotrimerization reaction of m-diethynylbenzene (DEB) (refs. 2-7). The cyclotrimerization of DEB is shown in Fig.1; further cyclotrimerization of available ethynyl groups results in products with increasing molecular weight. One of the PAA composites contained an additional component, poly(phenylquinoxaline) (PPQ), which was added to increase the toughness of the PAA matrix.

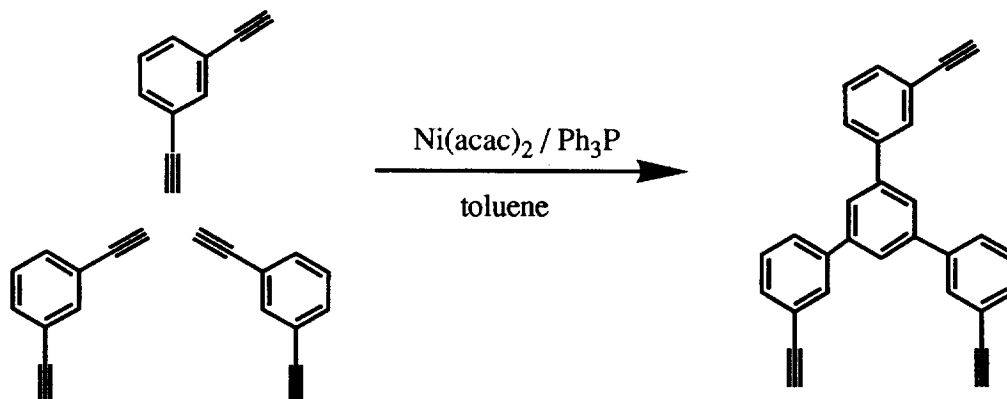


Figure 1. Cyclotrimerization reaction of diethynylbenzene (DEB).

The carbon fabric, designated T300, was from Ferro Corporation. HA-43 is a commercial version of PAA that was supplied by Hercules, Inc. PAA for panel B was prepared in toluene solution from m-diethynylbenzene and 1,4-diphenylbutadiyne in a manner analogous to that of Jabloner (ref. 2). PPQ for the panel C was prepared in m-cresol by the condensation reaction of bis-benzil and 3,3',4,4'-tetraaminobiphenyl (see Ref. 8 for details). The prepreg plies were prepared by impregnation of the carbon fabric with a toluene solution of the resin, followed by drying in air to evaporate the solvent. Formulation of the composite panels, which measured 3.8 cm x 8.8 cm x 0.3 cm, was as follows:

Panel A, HA-43/T300. Thirteen prepreg plies of HA-43/T300 were laid up and cured in a press at 3.4×10^6 Pa (500 psi) and 177°C for three hours, then allowed to cool to room temperature. Resin content of the panel was about 37 wt%. The panel was cut to provide leading and trailing edge samples designated L-A and T-A, respectively.

Panel B, PAA/T300. Thirteen prepreg plies of PAA/T300 were laid up and cured in a press at 3.4×10^6 Pa (500 psi) and 177°C for three hours, then allowed to cool to room temperature. Resin content of the panel was about 22 wt%. The panel was cut to provide leading and trailing edge samples designated L-B and T-B, respectively.

Panel C, HA-43, PPQ blend/T300. A resin mixture consisting of 86 g of dry HA-43, 86 g of dry PPQ, 2300 g of chloroform, 207 g of 1,1,1-trichloroethane, and 22 g of m-cresol was prepared to make the prepreg plies. Thirteen prepreg plies were laid up and cured in a press at 6.9×10^6 Pa (1000 psi) and 250°C for six hours, then allowed to cool to room temperature. Resin content of the panel was about 33 wt%. The panel was cut to provide leading and trailing edge samples designated L-C and T-C, respectively.

The leading edge panels were located on Bay D of Row 9, and the trailing edge panels were located on Bay D of Row 3. Row 9 received about 8.7×10^{21} atoms/cm² of atomic oxygen fluence (ref. 9) and 11,200 equivalent sun hours of radiation exposure (ref. 10), Row 3, about 1.3×10^{17} atoms/cm² and 11,100 equivalent sun hours. The difference in atomic oxygen exposure between Row 9 and Row 3 was more than 4 orders of magnitude, but there was essentially no difference in radiation exposure. The side of the panel that was subjected to the space environment will be referred to as the "exposed" face, and the reverse side of the panel that was mounted flat against LDEF will be referred to as the "backside." The

backside of each panel functions as a convenient control for the exposed side since laboratory control samples were not available.

On-orbit photography of the samples by the crew of the space shuttle Columbia showed that the samples were intact and relatively undamaged. After examination and photography at Kennedy Space Center, the experiment trays were flown to Aerospace and deintegrated by Aerospace personnel. Deintegration and the initial, cursory examination of individual samples were performed in a class 10,000 clean room. The samples were then packaged into individual, closed boxes for storage between experiments.

Scanning Electron Microscopy/Energy Dispersive X-Ray Spectroscopy

Analyses were performed on the front and back surfaces of the three pairs of composites samples. Each sample was studied as received. No sample preparation was necessary except pump-down at high vacuum for about 24 hours before introduction to the SEM (due to the large size of these samples). A JEOL 840 SEM with an EDAX 9900 EDS system was used for this study. Electron micrographs were acquired using accelerating voltages ranging from 5 to 25 kV. EDS data were acquired using an accelerating voltage of 15 kV, which allowed for the acquisition of the lower atomic number elements such as carbon and oxygen while still exciting X-ray fluorescence from heavier elements.

X-Ray Photoelectron Spectroscopy

Preparation for surface analysis by XPS involved cutting a segment approximately 1.5 cm x 1.5 cm from one end of each composite sample. This was necessary because the original panels were too large to be accommodated by the VG Scientific ESCALAB MKII instrument used for the analyses. A dry cut of the samples minimized surface contamination from the sample preparation step. Each sample was mounted on top of a stub using four Ta foil tabs that were spot welded around the stub periphery. During analysis of each exposed surface, the backside was in contact only with the top 1.3 cm diameter rim of the stub. This minimized surface contact contamination of the backsides, so that each sample could be remounted for the comparative analysis of the backside.

The Al K α source was chosen for X-ray irradiation. Survey scans from 0 to 1100 eV binding energy were acquired to qualitatively determine the sample surface composition. High resolution elemental scans were subsequently run to obtain semiquantitative elemental analyses from peak area measurements and chemical state information from the details of binding energy and shape. Measured peak areas for all detected elements were corrected by elemental sensitivity factors before normalization to give surface mole percent. The quantitation error on a relative basis is $\leq 10\%$ for components > 1 mole %. Large uncertainties in the relative elemental sensitivity factors can introduce absolute errors of a factor of 2 or even greater. All elements of the periodic table except H and He can be detected by XPS. The detection limit is about 0.1 surface mole %, but spectral overlaps between large peaks and small peaks can make it impossible to detect minor components. Scanning electron beam imaging, used to set up the sample surface analysis area, helped avoid analysis of sample edge areas that were masked from line-of-sight exposure to the space environment by the mounting hardware.

Cross Sections

After examination by XPS, the 1.5 cm x 1.5 cm samples were embedded in epoxy, cut, and polished so that the cross section of the sample could be examined by optical microscopy and SEM. The

samples were evaporatively coated with several hundred angstroms of carbon before SEM analysis. Average erosion depth measurements were made from the cross-section micrographs.

RESULTS AND DISCUSSION

Microscopy

The initial visual and light microscopy examinations of the samples showed that none of the composites had been catastrophically damaged by nearly six years of exposure to the space environment. The effect of the large difference in atomic oxygen exposure between the leading and trailing edges is illustrated in Fig. 2, which shows SEM micrographs of L-A and T-A. In both of the micrographs, the right-hand side of the sample was masked from the effects of the space environment by the mounting hardware. In Fig. 2, the lack of surface charging on the exposed area of L-A relative to the masked area and relative to T-A in the SEM chamber demonstrates that the nonconductive matrix at the surface of the leading edge samples was removed by atomic oxygen erosion. In each sample pair, we found that the exposed area of the leading edge sample had little or no surface charging, indicating that the conductive carbon fibers were exposed. The trailing edge samples had extensive surface charging and were difficult to image because the nonconductive matrix had not been removed by erosion.

The erosion process resulted in a morphology on all the leading edge samples that is best visualized by examining the micrographs of the surface and of the cross-sectioned samples. Figure 2 shows that a leading edge exposed surface is characterized by large crevasses that have developed predominantly parallel to the long axis of the fibers. This emphasizes the weave pattern of the carbon fiber tows in the fabric. However, the surface SEM micrographs do not clearly elucidate the condition of the remaining exposed fibers, even at higher magnification, as seen in Fig. 3. The optical micrograph cross section of the L-A surface shown in Fig. 4a highlights the "peak and valley" morphology associated with crevasse development on the exposed surface. Note that crevasses parallel to the cut of the cross section may not be seen. The area on the left side of the optical micrograph, where the sample was masked, shows the relatively smooth preflight condition of the surface. Higher magnification SEM micrographs of the L-C cross section are shown in Figs. 5-6. They show that the crevasses traversed both fibers and matrix, and most appeared to have steep sides and a well-defined tip. The crevasses ranged from 10 to 100 μm in depth, and no undercutting of the matrix relative to the fibers was apparent along the sides of the crevasses.

At this point, it may be useful to distinguish between "cracks" and "crevasses." Cracks form when two previously united sections of the composite become separated. There is no net loss of material during crack formation. The cracks observed in the samples were probably caused by thermal stresses during molding or during flight. In contrast, crevasses resulted from removal of fiber and matrix material, and were characterized by sharp triangular cross sections. Crevasses were completely absent on trailing edge sample surfaces, suggesting that they developed on leading edge surfaces as a result of atomic oxygen erosion. Figure 5 shows a section of L-C that contains both a surface crack and surface crevasses. The crack is narrow, uniform in width, and extends further into the sample interior than the wider, triangular crevasses. Note that the intersection of the crack with the surface did not cause a crevasse to form. In general, we found no correlation between the location of cracks and crevasses, and, as seen in Fig. 5, crevasses were more numerous than cracks.

It was estimated from the cross-section optical micrographs that the erosion depth on L-A and on L-C was about 125 μm . The measurements were taken at the left side of the micrographs (see Fig. 4), where there is an edge between the masked and exposed areas of the surface. Individual crevasses reflect erosion depths less than or greater than the value at the edge. The optical micrograph of L-B, shown in Fig. 4b, showed features similar to those in the micrographs of L-A and L-C. However, the average depth of erosion from Fig. 4b appeared to be 25 to 50 μm , and was difficult to measure because of the

curvature of the surface. For comparison, reactive polymers, such as Kapton and Mylar, were eroded to a relatively uniform depth of about 220 μm by the atomic oxygen fluence received on Row 9 (ref. 11). We hypothesize that the decreased erosion of the composites relative to polymers is probably best understood in terms of a two-step erosion process. In the first step, the outer layer of organic matrix was removed at roughly the same rate as other reactive polymers. In the second step, when the carbon fibers became exposed, a lower reaction efficiency for the fibers led to a lower overall (bulk) erosion rate, and contributed to the development of the highly irregular surface morphology. Carbon fabric/organic matrix composites with epoxy, polyimide, and polysulfone matrices were reported to have leading edge erosion values near the masked edge of 50 μm , 75 μm , and 50 μm , respectively (ref. 12), measured from cross section optical micrographs. Maximum crevasse depths of 80 μm were reported for the epoxy and polysulfone matrices, and 120 μm for polyimide matrices.

The addition of PPQ to the HA-43 matrix did not have an obvious effect on the erosion rate or pattern of erosion for L-C relative to L-A. L-B, however, was eroded only 20 to 40% as deeply as the other two composites, as seen by comparing Fig. 4b to 4a. Examination of L-B at high magnification, as seen in Fig. 7, revealed well-defined crevasses comparable to those on L-A and L-C in appearance, but on average less enlarged. The panel for samples L-B and T-B, fabricated using PAA prepared in our laboratory, had the lowest resin content (about 40% lower than the other two panels). In this case, the lower reaction efficiency of the fibers relative to the organic matrix would contribute to the lower erosion rate observed for L-B. With so few samples, it can only be noted at this point that resin content and/or the details of resin composition/fabrication may play an important role in the overall composite erosion rate.

Atomic oxygen exposure of epoxy-resin-embedded fibers on shuttle mission STS-8 resulted in much faster removal of epoxy from between the fibers than erosion of the fibers themselves (ref. 13). Nothing observed on the STS-8 samples led to a prediction that atomic oxygen erosion of composite surfaces would cause the highly defined crevasses observed on the LDEF-exposed composites. From STS-8 results, we would have predicted an erosion process that preferentially removed matrix, perhaps with significant undercutting of the matrix around fibers from atomic oxygen scatter in the eroded areas. The sharpness of the crevasse tips shown penetrating into the fibers in Fig. 6 was unexpected. Unlike the LDEF samples, the exposed fibers on STS-8 were metallographically prepared in the transverse direction; it is possible that fiber orientation plays an important role in the erosion process. On a macroscopic level, examination of the eroded composite surfaces showed a definite pattern correlated with fiber direction. This indicates that the carbon fibers are playing a crucial role in crevasse initiation and/or enlargement since a more uniform erosion pattern would be predicted, such as observed for graphite (ref. 13), or Teflon (ref. 14), if there were no differences in rate or mechanism between the atomic oxygen erosion of fibers and matrix. The possible role of preflight and on-flight contamination in crevasse initiation and enlargement is unknown at this time.

From these results, it seems clear that it is very difficult to predict the erosion morphology of composites from information obtained on relatively short shuttle missions. LDEF was subjected to thousands of thermal cycles, much higher levels of UV radiation, and a much higher atomic oxygen fluence than the samples that were exposed on shuttle mission STS-8. The relative importance of each of these factors and combinations thereof is presently unknown.

Energy Dispersive X-Ray Spectroscopy

At 15 kV, X-ray information for EDS surface composition determination comes from a depth of $\leq 1 \mu\text{m}$. The EDS data showed that all of the composites flown on LDEF were contaminated with Si and O. Low levels of Cl and Cu were also present on most of the analyzed samples. Other minor contaminants detected on one or more surfaces included Ca, Al, S, P, Mg, Ni, Fe, and Ti. In each case, the O concentration was higher on the exposed face than on the backside face, and higher on the leading edge exposed surface than on the trailing edge exposed surface, as seen in Fig. 8a. EDS data are not readily quantified for the low atomic number elements, such as C and O. Therefore, comparison of relative

surface concentrations has been approximated for these composite samples by using elemental peak heights (arbitrary units) after setting all of the carbon peaks to the same height. This should be a valid approximation since carbon from the fabric and organic matrix is the dominant component in the volume analyzed (SEM analysis of the sample cross sections and XPS analyses do not show thick contaminant overlayers on the exposed surfaces). It is seen in Fig. 8b that the silicon concentration was higher on the leading edge exposed surfaces than on the trailing edge exposed surfaces or any of the backside surfaces. The exposed surface of L-B had higher silicon and oxygen concentrations than the exposed surfaces of L-A and L-C, which is consistent with the lower extent of erosion on L-B observed in the micrographs.

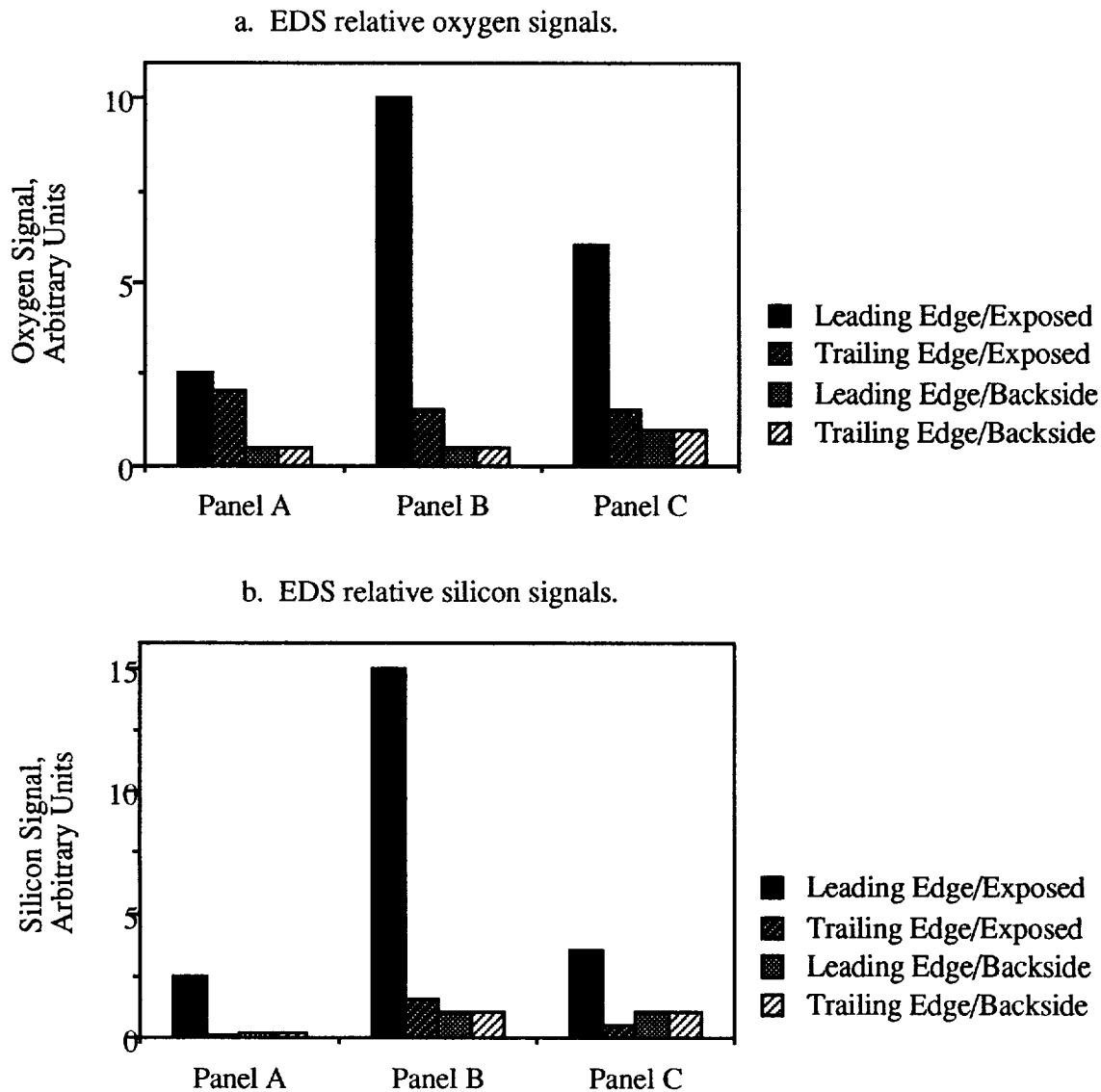


Figure 8. EDS surface composition of samples compared as a function of exposure.

X-Ray Photoelectron Spectroscopy

The XPS surface composition results are tabulated in Table I. The experimental depth of analysis was about 50 to 100 Å. Since this depth is roughly 1% of the depth probed by EDS analysis, XPS is much more sensitive to surface contaminants and less sensitive to bulk compositional differences.

Table I. XPS Data for LDEF Fiber/Organic Matrix Composites

Sample ID	Sample Surface	Surface Mole %, Normalized ^a													
		C	O	Si	N	F	S	Cl	Cu	Zn	Ni	Sn	Na	P	
L-A	Exposed	45	42	10	2		0.6		0.3						
	Exposed	44	44	8	1	0.4	0.5	tr	2	0.3					
	Backside	71	20	2	2	3	0.1	0.1	1	tr					
T-A	Exposed	51	36	6	2	3	tr	0.1	3	0.2		0.1			
	Backside	66	26	2	1	3	0.2	0.1	1						
L-B	Exposed	17	59	19	0.6	nd	0.3	0.1	2	tr	1		nd	0.3	
	Backside	59	31	3	2	2	0.2	0.2	2	nd			1	nd	
T-B	Exposed	45	23	4	0.9	25	0.1	0.1	1	0.1			0.1		
	Exposed	46	27	3	1	19	0.1	0.2	2	0.2			1		
	Backside	70	22	2	1	3	0.1	0.2	0.7	nd			0.2	nd	
L-C	Exposed	61	31	3	3	0.1	0.5	nd	0.3	nd		0.4	0.3	0.6	
	Backside	67	23	4	2	3	0.1	0.2	2	nd		nd	0.1	nd	
T-C	Exposed	47	39	7	2	0.4	0.2	0.4	5	0.4		tr	0.1	nd	
	Backside	65	24	4	1	0.3	nd	0.3	1	0.2		tr	nd	nd	
Release Cloth		39	4	0.7		56									

^atr = trace.

nd = not detected in elemental scan.

blank = not detected in survey scan and no elemental scan acquired.

Examination of the data in Table I shows that the surface composition of the fiber/organic matrix composites is complex, but the major surface contaminants are silicon and oxygen. For five of the six samples, the exposed vs. backside surface comparison reveals significantly higher silicon on the exposed surfaces. The concentration of silicon ranged from 3 to 19 mole % on the exposed surfaces, and from 2 to 4 mole % on the backsides. The backsides have probably accumulated some surface contamination on flight (ref. 15). The exposed surface oxygen concentration on each of the samples is higher and the carbon concentration is lower relative to the backside surface. The decrease in carbon concentration on the exposed surfaces is due to attenuation of the carbon fabric/organic matrix signals by contaminant buildup.

The predominant surface species of Si on the exposed surfaces was SiO₂, based on a measured binding energy for the Si2p peaks of about 103.5 eV. The silicon detected on the sample backsides was predominantly from silicone or mixed silicone/silicate/silica, based on a measured binding energy for the Si2p peaks of ≤103.0 eV. SiO₂ is generally accepted to be a degradation product from silicones outgassed

from materials on LDEF such as RTV silicones (ref. 16). Atomic oxygen reactions and UV radiation damage could cause degradation of silicones. It is probable that the return flux from atmospheric backscatter, i.e., collisions with residual atmosphere such as atomic oxygen, resulted in enhanced deposition of silicones and other contaminants on the leading edge flight surfaces relative to the trailing edge. The exposed surface of L-B had higher silicon and oxygen concentrations than the exposed surfaces of L-A and L-C, which is consistent with the lower extent of erosion observed in the micrograph of L-B. It is not known what role the buildup of contamination layers may have had on crevasse initiation and enlargement during atomic oxygen erosion of the leading edge surfaces.

A significant fraction of the surface carbon detected may be due to contamination residues from outgassed silicones or hydrocarbons, but XPS did not differentiate contamination from the composite surface components in this complex system. The inability to discriminate between deposited carbon contamination and the composite matrix also makes it impossible with these data to assess chemical changes induced in the composite surfaces by space environment exposure. XPS analysis of contamination on a variety of materials from LDEF (ref. 15) showed that in general the silicon contamination levels were higher on the leading edge surfaces than on the trailing edge surfaces, and that the trailing edge deposits contained a higher percentage of carbon than the leading edge deposits. It was hypothesized in ref. 16 that atomic oxygen reactions volatilized carbon from the leading edge surface residues, leaving predominantly SiO₂. The XPS analyses, however, did not conclusively show different relative total thicknesses of flight-deposited contamination for leading and trailing edge surfaces. The data were consistent with a contaminant film that has an average thickness of 50 to 100 Å. The contaminant overlayer is probably patchy, with significant areas covered by less than 100 Å, and other areas by greater than 100 Å of molecular film.

A major concentration of degraded fluorocarbon (as indicated by about 20 mole % F) was detected on the exposed surface of sample T-B. At least minor concentrations were observed on all but one sample surface. The observed fluorine contamination levels on other LDEF surfaces analyzed by XPS, including paints, Kapton, and aluminum alloy composites, have been <1 mole %. It is probable that some of the carbon/organic matrix composite surfaces have high residual fluorocarbon residue from the release cloth used in their fabrication. The surface composition of a sample of release cloth is included at the bottom of Table I.

The minor surface contaminants detected on the composite surfaces included N, S, Cl, and Cu on most of the analyzed surfaces and Zn, Ni, Sn, Na, and P on one or more surfaces. For all contaminants except silicon and oxygen, the exposed surface is not consistently different from the backside. Preflight contamination of this type is normal for complex materials and is considered the most significant source for the minor contaminants. The exposed flight surfaces were not contaminated with detectable levels of ⁷Be as measured by XPS or EDS. The detected concentrations of ⁷Be on other LDEF exposed surfaces were about 1-10 parts per billion (ref. 17), well below the detection limits of XPS and EDS.

CONCLUSIONS

None of the composites were catastrophically damaged by nearly six years of exposure to the space environment. The trailing edge samples exhibited no physical appearance changes due to exposure. Composites on the leading edge were eroded to a depth from 25 to 125 μm. More quantitative measures of the erosion level were difficult because of the irregularity of the erosion process. The erosion morphology was dominated by crevasses parallel to the fibers with triangular cross sections 10-100 μm in depth. The location of the crevasses was not correlated with the location of surface cracks. The edges of the crevasses were well defined and penetrated through both matrix and fiber. No preferential removal of the matrix relative to the fibers was apparent along the sides in the crevasse enlargement pattern. At the present time, we do not know the mechanism for the formation of the crevasses. However, the data suggest that the carbon fibers are playing an important role in crevasse initiation and/or enlargement, and in the overall

erosion rate. The available data did not lead to a conclusion that there are differences in erosion behavior between matrix types, but resin content and/or the details of resin composition/fabrication may play a role in determining the overall composite erosion rate.

It is difficult to predict long-term atomic oxygen erosion morphology of composite materials from erosion data obtained on short shuttle missions. A better understanding of other factors, such as thermal cycling and UV exposure, that may influence erosion is necessary to improve the accuracy of these predictions.

Major on-flight contamination from silicones was observed, as evidenced by higher levels of silicon and oxygen detected on the exposed surfaces than on the backsides. Silicon and oxygen contamination levels were higher on the leading edge surfaces than on the trailing edge surfaces. It is probable that the return flux associated with atmospheric backscatter resulted in enhanced deposition of silicones and other contaminants on the leading edge flight surfaces. The exposed surface of PAA/T300 had higher silicon and oxygen concentrations than the exposed surfaces of HA-43/T300 and HA-43, PPQ blend/T300, which is consistent with the lower extent of erosion observed on PAA/T300. The role of contamination in crevasse initiation and enlargement is unknown at this time. Good agreement was seen between EDS and XPS data on major contaminants, with minor differences explained by the difference in depth probed by the two techniques. The presence of a wide range of minor contaminants, probably due to preflight contamination, was also observed.

ACKNOWLEDGMENTS

This experiment was initially conceived by Dr. James Gee, Camille Gaulin, and Clark Williams. The LDEF deintegration effort was performed by Sandra Gyetvay, Laana Fishman, and Dr. Michael Meshishnek, with funding from the Space Test Program (administered by the Air Force SSD/CLP). The initial examination and photography of the composite samples were performed by Sandra Gyetvay, Laana Fishman, and Dr. Michael Meshishnek, with funding from SDIO/TNK under the Space Environment Effects (SEE) Program, administered by Wright Laboratory Materials Directorate. The authors would like to credit Mr. Ca Su with the preparation of the cross-section samples. We would also like to thank Dr. Sherrie Zacharius, Dr. Howard Katzman, Dr. Gary Steckel, Dr. Gerald Rellick, and Dr. Wayne Stuckey for helpful suggestions and comments. This work was supported by the Wright Laboratory Materials Directorate and by The Aerospace Corporation Mission Oriented Investigation and Experimentation program.

REFERENCES

1. Schall, P.: Space Environment Effects on Spacecraft Materials (M0003). *The Long Duration Exposure Facility (LDEF). Mission 1 Experiments*, NASA SP-473, 1984, pp. 44-48.
2. Jabloner, H.: Poly(arylacetylene) Molding Compositions. U. S. Patent No. 4,070,333, 1978.
3. Whitesides, G. M.; and Neenan, T. X.: Synthesis of High Carbon Materials from Acetylenic Precursors. Preparation of Aromatic Monomers Bearing Multiple Ethynyl Groups. *J. Org. Chem.*, vol. 53, no. 11, 1988, pp. 2489-2496.
4. Barry, W. T.; Gaulin, C. A.; and Kobayshi, R. W.: Review of Polyarylacetylene Matrices for Thin-Walled Composites. The Aerospace Corporation, El Segundo CA, TR-0089(4935-06)-1, Sept. 1989.

5. Katzman, H. A.: Polyarylacetylene Resin Composites. The Aerospace Corporation, El Segundo CA, TR-0090(5935-06)-1, April 1990.
6. Zaldivar, R. J.; Rellick, G. S.; and Yang, J. M.: Processing Effects on the Mechanical Behavior of Polyarylacetylene-Derived C-C. *Sampe J.*, vol. 27, no.5, 1991, pp. 29-36.
7. Zaldivar, R. J.; Kobayashi, R. W.; Rellick, G. S.; and Yang, J. M.: Carborane-Catalyzed Graphitization in Poly(arylacetylene)-Derived Carbon-Carbon Composites. *Carbon*, vol. 29, no. 8, 1991, p. 1145-1153.
8. Hergenrother, P. M.: Polyphenyl Quinoxilines: Synthesis, Characterization, and Mechanical Properties. *J. Appl. Polym. Sci.*, vol. 18, 1974, pp. 1779-1791.
9. Bourassa, R. J.; and Gillis, J. R.: Atomic Oxygen Exposure of LDEF Experiment Trays. NASA CR-189627, May 1992.
10. Bourassa, R. J.; and Gillis, J. R.: Solar Exposure of LDEF Experiment Trays. NASA CR-189554, Feb. 1992.
11. Gregory, J. C.: Atomic Oxygen Erosion Yields of LDEF Materials. Presented at the LDEF Materials Workshop '91, Hampton VA, Nov. 1991.
12. George, P. E.; and Hill, S. G.: Results from Analysis of Boeing Composite Specimens Flown on LDEF Experiment M0003. *NASA/SDIO Space Environmental Effects on Materials Workshop*, NASA CP-3035, Part 2, June, 1988, pp. 1115-1141.
13. Meshishnek, M. J.; Stuckey, W. K.; Evangelides, J. S.; Feldman, L. A.; Peterson, R. V.; Arnold, G. S.; and Peplinski, D. R.: Effects on Advanced Materials: Results of the STS-8 EOIM Experiment. The Aerospace Corporation, El Segundo, CA, TR-0086(6935-05)-2, July 1987.
14. Hemminger, C. S.; Stuckey, W. K.; and Uht, J. C.: Space Environmental Effects on Silvered Teflon Thermal Control Surfaces. *LDEF--69 Months in Space. First Post-Retrieval Symposium*, NASA CP-3134, Part 2, June, 1991, pp. 831-845.
15. Hemminger, C. S.: Surface Contamination on LDEF Exposed Materials. Presented at the LDEF Materials Workshop '91, Hampton VA, Nov. 1991.
16. Crutcher, E. R.; and Warner, K. J.: Molecular Films Associated with LDEF. *LDEF--69 Months in Space. First Post-Retrieval Symposium*, NASA CP-3134, Part 1, June, 1991, pp. 155-177.
17. Fishman, G. J.; Harmon, B. A.; Gregory, J. C.; Parnell, T. A.; Peters, P.; Phillips, G. W.; King, S. E.; August, R. V.; Ritter, J. C.; Cutchin, J. H.; Haskins, P. S.; McKisson, J. E.; Ely, D. W.; Weisenberger, A. G.; Piercey, R. B.; and Dybler, T.: Observation of ^7Be on the Surface of LDEF Spacecraft. *Nature*, vol. 349, no. 6311, 1991, pp. 678-80.

EXPOSED

MASKED



(a)

EXPOSED

MASKED



(b)

Figure 2. Difference in surface erosion of samples after leading and trailing edge exposure. (a) SEM of sample L-A surface; (b) SEM of sample T-A surface.

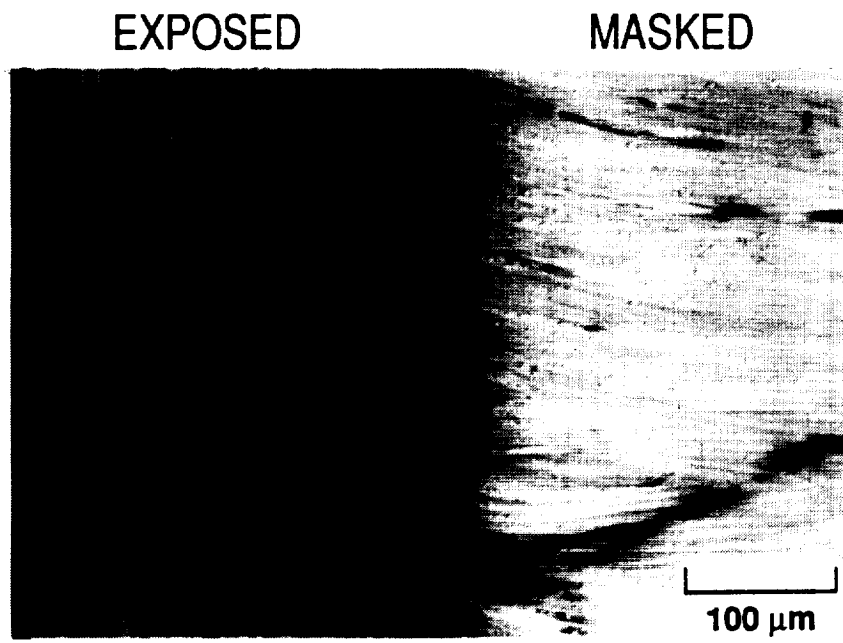


Figure 3. SEM micrograph of L-C surface showing details of exposed and masked areas.

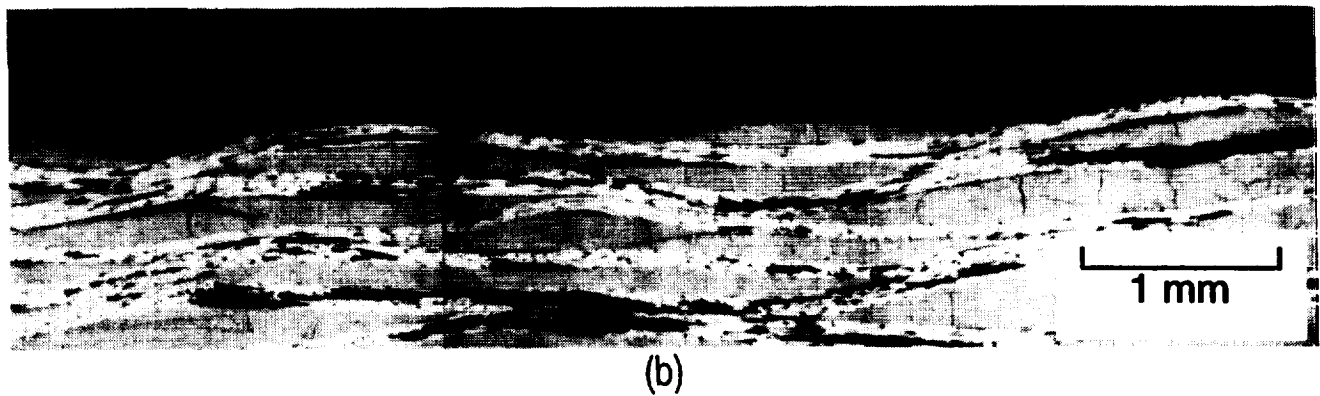
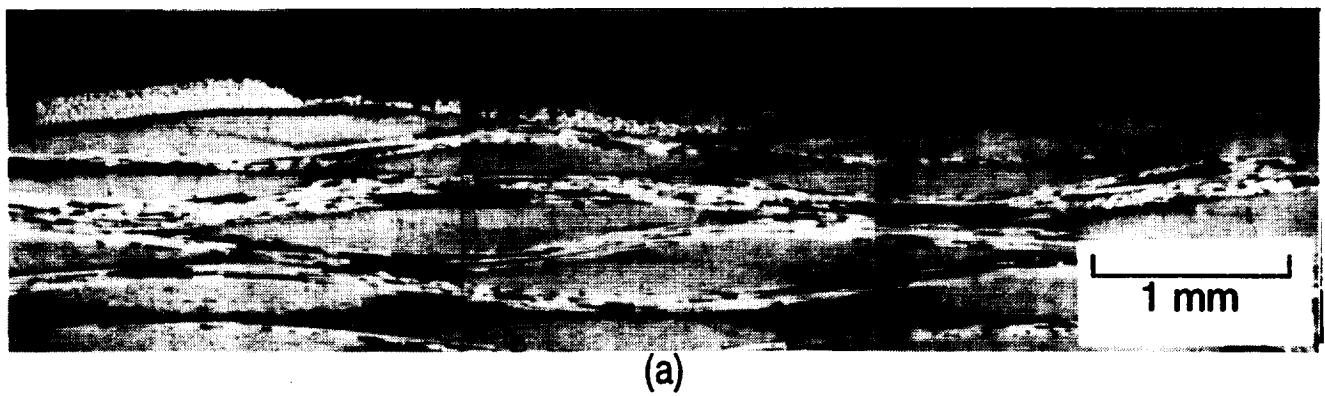


Figure 4. Optical micrographs of (a) L-A cross section and (b) L-B cross section.

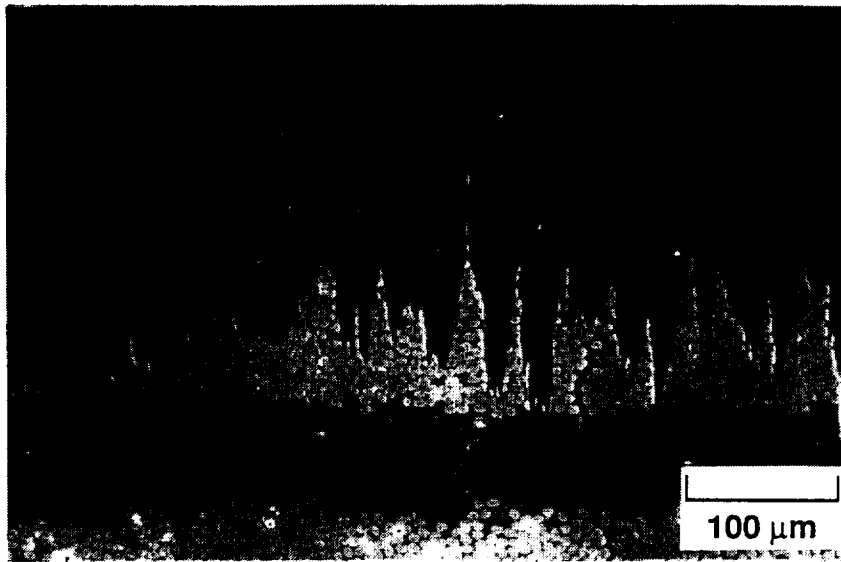


Figure 5. SEM micrograph of L-C cross section contrasting surface crack with surface crevasses .

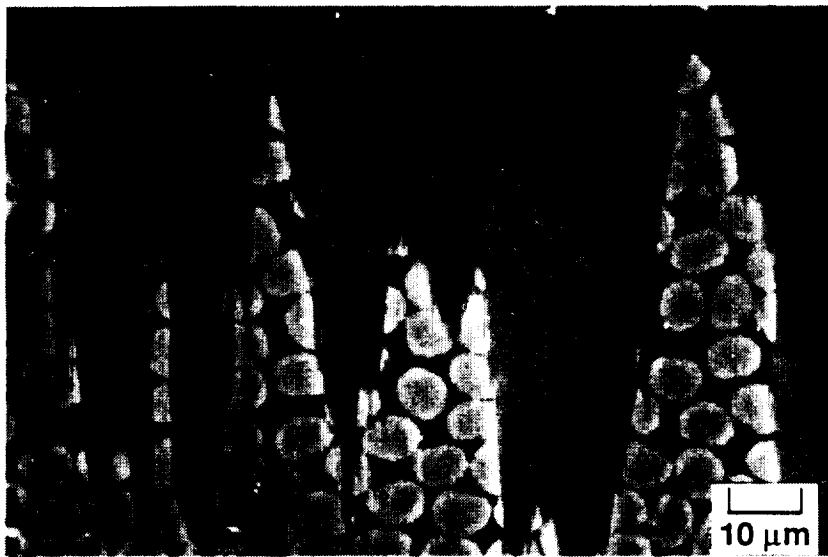


Figure 6. SEM micrograph of detail of L-C cross section.

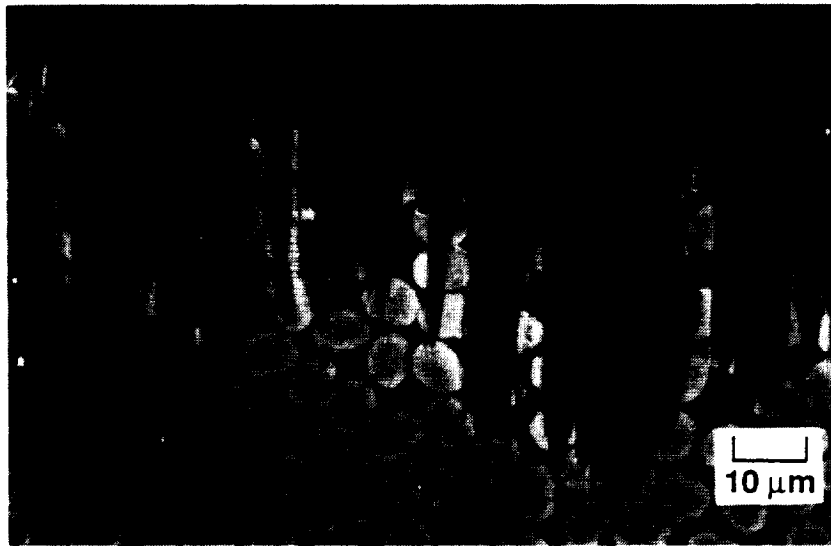


Figure 7. SEM micrograph of detail of L-B cross section.